Neurobiology of Disease 130 (2019) 104509

Contents lists available at ScienceDirect

Neurobiology of Disease

journal homepage: www.elsevier.com/locate/ynbdi

Proteomic signatures of brain regions affected by tau pathology in early and late stages of Alzheimer's disease

Clarissa Ferolla Mendonça[a,b], Magdalena Kuras[c], Fábio César Sousa Nogueira[a,d], Indira Plá[c], Tibor Hortobágyi[e,f,g], László Csiba[e,h], Miklós Palkovits[i], Éva Renner[i], Péter Döme[j,k], György Marko-Varga[c], Gilberto B. Domont[a,*], Melinda Rezeli[c,*]

[a] Proteomics Unit, Department of Biochemistry, Federal University of Rio de Janeiro, Rio de Janeiro, Brazil
[b] Gladstone Institute of Neurological Disease, San Francisco, USA
[c] Division of Clinical Protein Science & Imaging, Department of Clinical Sciences (Lund) and Department of Biomedical Engineering, Lund University, Lund, Sweden
[d] Laboratory of Proteomics, LADETEC, Institute of Chemistry, Federal University of Rio de Janeiro, Rio de Janeiro, Brazil
[e] MTA-DE Cerebrovascular and Neurodegenerative Research Group, University of Debrecen, Debrecen, Hungary
[f] Institute of Pathology, Faculty of Medicine, University of Szeged, Szeged, Hungary
[g] Centre for Age-Related Medicine, SESAM, Stavanger University Hospital, Stavanger, Norway
[h] Department of Neurology, Faculty of Medicine, University of Debrecen, Debrecen, Hungary
[i] SE-NAP – Human Brain Tissue Bank Microdissection Laboratory, Semmelweis University, Budapest, Hungary
[j] Department of Psychiatry and Psychotherapy, Semmelweis University, Budapest, Hungary
[k] National Institute of Psychiatry and Addictions, Nyírő Gyula Hospital, Budapest, Hungary

ARTICLE INFO

Keywords:
Alzheimer's disease
Proteomics
Brain region vulnerability
Medial temporal lobe
Neocortex
Braak/Braak staging

ABSTRACT

Background: Alzheimer's disease (AD) is the most common neurodegenerative disorder. Depositions of amyloid β peptide (Aβ) and tau protein are among the major pathological hallmarks of AD. Aβ and tau burden follows predictable spatial patterns during the progression of AD. Nevertheless, it remains obscure why certain brain regions are more vulnerable than others; to investigate this and dysregulated pathways during AD progression, a mass spectrometry-based proteomics study was performed.

Methods: In total 103 tissue samples from regions early (entorhinal and parahippocampal cortices - medial temporal lobe (MTL)) and late affected (temporal and frontal cortices - neocortex) by tau pathology were subjected to label-free quantitative proteomics analysis.

Results: Considering dysregulated proteins during AD progression, the majority (625 out of 737 proteins) was region specific, while some proteins were shared between regions (101 proteins altered in two areas and 11 proteins altered in three areas). Analogously, many dysregulated pathways during disease progression were exclusive to certain regions, but a few pathways altered in two or more areas. Changes in protein expression indicate that synapse loss occurred in all analyzed regions, while translation dysregulation was preponderant in entorhinal, parahippocampal and frontal cortices. Oxidative phosphorylation impairment was prominent in MTL. Differential proteomic analysis of brain areas in health state (controls) showed higher metabolism and increased expression of AD-related proteins in the MTL compared to the neocortex. In addition, several proteins that differentiate brain regions in control tissue were dysregulated in AD.

Conclusions: This work provides the comparison of proteomic changes in brain regions affected by tau pathology at different stages of AD. Although we identified commonly regulated proteins and pathways during disease advancement, we found that the dysregulated processes are predominantly region specific. In addition, a distinct proteomic signature was found between MTL and neocortex in healthy subjects that might be related to AD

Abbreviations: AD, Alzheimer's disease; EC, Entorhinal cortex; PHC, Parahippocampal cortex; TC, Temporal cortex; FC, Frontal cortex; MTL, Medial temporal lobe; NFT, Neurofibrillary tangles; Aβ, Amyloid β peptide; CBD, Corticobasal degeneration; PSP, Progressive supranuclear palsy; DEP, Differentially expressed protein; AMBIC, Ammonium-bicarbonate; DTT, Dithiothreitol; IAA, Iodoacetamide; TFA, Trifluoroacetic acid

* Corresponding authors at: Gilberto B. Domont, Proteomics Unit, Department of Biochemistry, Federal University of Rio de Janeiro, Rio de Janeiro, Brazil; Melinda Rezeli, Division of Clinical Protein Science & Imaging, Department of Clinical Sciences (Lund) and Department of Biomedical Engineering, Lund University, Lund, Sweden.

E-mail addresses: gilbertodomont@gmail.com (G.B. Domont), melinda.rezeli@bme.lth.se (M. Rezeli).

https://doi.org/10.1016/j.nbd.2019.104509
Received 27 December 2018; Received in revised form 17 May 2019
Available online 15 June 2019

vulnerability. These findings highlight the need for investigating AD's cascade of events throughout the whole brain and studies spanning more brain areas are required to better understand AD etiology and region vulnerability to disease.

1. Introduction

Alzheimer's disease (AD) is the most prevalent neurodegenerative disorder and also the major cause of dementia (60–80% cases) (Alzheimer's Association, A. S, 2017). Major hallmarks of AD are loss of synapses, neuronal death and deposition of extracellular amyloid β peptide (Aβ) and intracellular hyperphosphorylated tau protein (Masters et al., 2015). During AD progression Aβ and tau aggregates spread through the brain, following predictable patterns (Braak and Braak, 1991; Thal et al., 2002). Tau deposition was classified into six neuropathological stages designated as Braak/Braak (B/B) stages (Braak and Braak, 1991). During B/B I-II, tau inclusions are restricted to the transentorhinal and entorhinal cortices. They disseminate into the limbic system during B/B III-IV with the mild engagement of the hippocampus (CA1–4), parts of the frontal and temporal neocortices and the amygdala. The final stages, B/B V-VI, are distinguished by the destruction of the neocortex by protein inclusions (Hyman et al., 2012). There is a correlation between cognitive impairment and the number of neuritic plaques (Aβ plaques) in the neocortex, but cortical tau neurofibrillary tangles (NFT) burden correlates better with cognitive decline (Nelson et al., 2007).

Since AD progressively affects distinct brain regions, many studies compared the changes that occur in different regions, trying to elucidate which processes make an area more vulnerable than another one (Martin et al., 2008; Schonberger et al., 2001; Xu et al., 2019; Zahid et al., 2014). Other authors focused on the temporal advancement of AD by investigating changes that occur in one brain area at different disease stages (Bossers et al., 2010; Hondius et al., 2016; Kim et al., 2018; Lachén-Montes et al., 2017; Lau et al., 2013; Sultana et al., 2010; Triplett et al., 2016; Zelaya et al., 2015). Both strategies were also merged through transcriptomic/proteomic investigation of brain areas considering distinct disease stages (Matarin et al., 2015; McKetney et al., 2019; Miyashita et al., 2014; Savas et al., 2017; Seyfried et al., 2017).

Although many works have profiled molecular alterations in the AD brain, a large human study investigating proteomic changes at different B/B stages in brain areas vulnerable and resilient to tau pathology is still lacking. With the aim to map proteome dysregulation during AD progression in brain regions with distinct susceptibility to neurodegeneration and to investigate which processes make some brain areas more vulnerable to AD, we performed quantitative proteome profiling of 103 human brain samples from regions affected by tau pathology already in the early (medial temporal lobe (MTL)) or only the late stages of AD (neocortex).

2. Methods

2.1. Patient cohort

A total of 103 postmortem human brain samples from 4 distinct brain regions (entorhinal cortex (Brodmann areas 28 and 34), parahippocampal cortex (posterior two thirds of the parahippocampal gyrus), temporal cortex (Brodmann area 21) and frontal cortex (Brodmann area 10)) were acquired from the Human Brain Tissue Bank (Semmelweis University, Budapest, Hungary). All brains were diagnosed by a neuropathologist according to the standard diagnostic criteria as described previously (Skogseth et al., 2017). In brief, the neuropathological diagnosis of AD was established when AD-type tau pathology was present in forms of neurofibrillary tangles, neuropil threads and Alzheimer's type (neuritic) plaques with coexisting characteristic amyloid beta pathology. The probability of AD is based on tau Braak & Braak (B/B) stage. Pure AD cases have been selected, i.e. brains without significant coexisting non-AD pathologies such as FTLD-tau, PSP, CBD. Cases were classified according to tau pathology (B/B stages) into controls (negative or minimal age-related tau pathology) and B/B stages (I, II, III, IV, V and VI) (Table S1). The work has been carried out in accordance with the Declaration of Helsinki. Brains were donated under informed written consent.

2.2. Microdissection procedure

After dissecting the whole brain from the skull, the leptomeninges were first removed from the surface of the brain. Subsequently, the cortex with the diencephalon was separated from the lower brainstem/cerebellum by a knife cut through the midbrain. Then, the cortex was sliced at the coronal level from the frontal pole with 1.5–2.0 cm thick sections. Each section (generally 11–12 from the whole brain) was immediately frozen individually on dry ice powder, covered in aluminum foil and stored at −70 °C. During the microdissection of the cortical samples, each frozen coronal section was further cut into 1–2 mm thin sections and the cortical areas were dissected out by the "micropunch technique" (Palkovits, 1973) using special micropunch needles with various (0.5–3.0 mm) inside diameters according to the size of the cortical areas or regions to be dissected. The microdissected tissue pellets were collected in 1.5 ml Eppendorf tubes and kept until use at −70 °C. During each step of the microdissection procedure, the brain slices and samples were kept frozen. For the present study, samples were taken from the entorhinal and parahippocampal cortex, the temporal cortex represented by micropunches from the middle temporal gyrus, and the frontal cortex by samples from the superior frontal gyrus.

2.3. Reagents

All reagents used were acquired from Sigma-Aldrich unless specified. Organic solvents and water with LC-MS quality were bought from Merck.

2.4. Protein extraction and digestion

The microdissected frozen tissue samples were sectioned at −20 °C using a cryostat to obtain 10 µm slices (20–60 slices per sample) and samples were stored at −80 °C until further usage. 200 µL of lysis buffer (7 M urea, 2 M thiourea, 50 mM Tris pH 7.4, MS-SAFE protease inhibitor) was added to each microcentrifuge tube containing the tissue slices. Samples were vortexed and then sonicated on ice (Digital Branson Sonicator SFX 150): 20% amplitude, pulsed mode (9 pulses with 10 s each and intervals of 10 s between each pulse). Lysates were centrifuged at 21,000 xg at 4 °C for 30 min (Eppendorf Nordic A/S) and the supernatant was transferred to a new tube to avoid cell debris. Prior to digestion, protein quantification was done using the Bradford 96 well plate assay, according to the manufacturer instructions.

Protein digestion was carried out using a modified Filter Aided Sample Preparation (FASP) protocol (Wisniewski et al., 2009). 100 µg protein was used for digestion. Reduction of disulfide bonds was performed by the addition of 50 mM dithiothreitol (DTT) to the lysates that were then incubated for 1 h at 30 °C. The samples were then transferred to 30 kDa Microcon filters (Merck Millipore) connected to collection tubes. 200 µL of U/Tris buffer (8 M Urea in 0.1 M Tris-HCl pH 8.5) was added and the filter units were centrifuged at 12,000 xg for 15 min at

room temperature. For alkylation of the cysteine residues, 50 µL of 50 mM iodoacetamide (IAA) in U/Tris buffer was added to the samples and the reaction was incubated in dark for 20 min at room temperature. IAA was then removed from the samples by filtration at 12,000 x g for 15 min. After that, 100 µL of U/Tris buffer was added to the filters and another centrifugation step with the same conditions was carried out. Prior to digestion U/Tris buffer was replaced to ammonium bicarbonate buffer (AMBIC) by the addition of 100 µL of 50 mM AMBIC, followed by centrifugation 12,000 x*g* for 15 min. This step was repeated 4 times. Filters containing the proteins were transferred to new collection tubes and 50 µL of 0.04 µg/uL sequencing grade modified trypsin (1:50 enzyme: protein ratio, Promega Biotech AB, Madison, WI) in AMBIC was added to each sample. Following overnight digestion at 37 °C, the peptides were collected by centrifugation at 12,000 x*g* for 15 min. Two elution steps were carried out by the addition of 100 uL of AMBIC, followed by centrifugation. Formic acid was added to a final concentration of 0.5%. Peptides were dried with speed vacuum centrifugation, then resuspended in 100 µL of 0.1% trifluoroacetic acid (TFA) and finally desalted by reversed phase chromatography using C18 spin columns (*MacroSpin Columns®*, The Nest Group Inc.). After desalting, tryptic peptides were dried and resuspended in 50 µL of 0.1% formic acid. Prior to injection onto the mass spectrometer, peptides were quantified using the Pierce Quantitative Colorimetric Peptide Assay (Thermo Fisher Scientific, Rockford, lL).

2.5. Liquid chromatography coupled to tandem mass spectrometry (LC-MS/MS)

1 µg of the tryptic peptides was injected for each analysis spiked with the Pierce retention time calibration mixture (PRTC) (Thermo Fisher Scientific, Rockford, lL) (25 fmol/injection). For LC-MS/MS analysis, we used a Thermo Q Exactive mass spectrometer (Thermo Scientific, Waltham, MA) equipped with a Dream ionization source (AMR Inc., Tokyo) and connected to an Easy n-LC 1000 liquid chromatography system (Thermo Scientific, Waltham, MA). Peptides were injected on an Acclaim PepMap 100 pre-column (100 µm × 2 cm, Thermo Fisher Scientific) and separated on a Zaplous α Pep-C18 analytical column (0.1 mm × 20 cm, AMR Inc., Tokyo) at a flow rate of 500 nL/min and a column temperature at 24 °C. A non-linear gradient was established using solvents A (0.1% formic acid in water) and B (0.1% formic acid in acetonitrile) to elute the peptides. The gradient started with 5% solvent B and increased to 22% during 100 min. In the next 14 min, solvent B increased to 32% and finally, it augmented to 95% in 12 min and it was kept at 95% for 14 min. Samples were analyzed using a top 15 data-dependent acquisition (DDA) method. MS1 scan was acquired in the Orbitrap analyzer with a 400–1600 *m/z* interval, 70,000 (@ 200 m/z) resolution, target AGC value of 1e6 and maximum injection time of 100 ms. The 15 most intense peaks (charge ≥2) were selected and fragmented in a Higher Energy Collisional Dissociation (HCD) cell with a normalized collision energy of 30%. MS2 spectra were acquired with a 17,500 (@ 200 m/z) resolution, target AGC value of 2e5 and maximum injection time of 120 ms. The ion selection threshold was set to 8.3e3 and dynamic exclusion was set to 20 s. Samples were randomly analyzed and each run was followed by a blank injection (0.1% formic acid in MilliQ water) with a short gradient of 35 min to avoid any residues from the previous sample. A quality control sample (QC) was prepared from a pool of 4 brain digests spiked with PRTC. 1 µg of QC sample together with 25 fmoles of PRTC peptides was injected after every 15 samples in order to evaluate system stability.

2.6. Protein inference and relative quantification

Raw data generated on the mass spectrometer was analyzed using the software Proteome Discoverer (PD) version 2.1 (Thermo Scientific, Waltham, MA). Peptide identification was done with the SEQUEST HT algorithm using the UniProt human database as reference (version from 07/09/2016, canonical sequences only). The following search parameters were employed: cysteine carbamidomethylation as static modification, methionine oxidation as dynamic modification, 10 ppm tolerance for precursor ions and 0.02 Da for fragment ions. A maximum of 2 missed cleavages was allowed. Protein quantification was done using the Precursor Ions Area Detector node, where the average of the 3 most intense peptides was used for protein quantification, being considered only unique peptides. The mass spectrometry proteomics data have been deposited to the ProteomeXchange Consortium via the PRIDE (Vizcaíno et al., 2015) partner repository with the dataset identifier PXD010138.

2.7. Targeted MS/MS analysis by parallel reaction monitoring (PRM)

Parallel reaction monitoring (PRM) was employed to verify a set of differentially expressed proteins. One to five unique peptides for each protein of interest were selected, and in the final assay, 75 peptides corresponding to 21 proteins (including apolipoprotein E2, E3, and E4 and a peptide associated with Aβ) were monitored (Table S2). The protein digests were spiked with a mixture of stable isotope standard peptides (SIS) correspond to apolipoprotein E (4 isoform-specific peptides and one peptide that is common in all isoforms). 1 µg of the tryptic peptides was injected for each analysis spiked with SIS peptides (20 fmoles/injection). For the PRM analysis, a Thermo Q Exactive HF-X mass spectrometer was used equipped with an Easy-spray source and connected to an UltiMate 3000 RSLCnano system (Thermo Scientific, Waltham, MA). Peptides were injected on an Acclaim PepMap 100 pre-column (75 µm × 2 cm, C18, 3 mm, 100 Å Thermo Scientific) and separated on an EASY-Spray column (75 µm × 25 cm, PepMap RSLC C18, 2 mm, 100 Å) at a flow rate of 300 nL/min and a column temperature at 45 °C. A non-linear gradient was established using solvents A (0.1% formic acid in water) and B (0.1% formic acid in 80% acetonitrile) to elute the peptides. The gradient started with 4% solvent B and increased to 30% in 30 min. In the next 5 min, solvent B increased to 45% and finally increased to 98% in 1 min and it was kept at 98% for 5 min.

Targeted MS2 mode was operated with the time-scheduled acquisition of the selected precursors with 3 min retention time windows. MS2 scans were acquired using 30,000 (@ 200 *m/z*) resolution, the AGC target value was set to 2e5 and 100 ms maximum injection time was used. Fragmentation was performed with a normalized collision energy of 27. Samples were randomly analyzed, and each run was followed by a blank injection to avoid any residues from the previous sample.

2.8. Bioinformatics and statistical analysis

Proteins identified from database search that fulfilled the following requirements were subjected to further analysis: master protein, 1% FDR, and identified with at least 2 peptides. Statistical analysis was carried out in Perseus v 1.6.0.7 and R. Protein area values were converted to log2 scale and normalized by subtracting the median of the sample distribution. Proteins with < 50% valid values in each group (controls, early and late B/B) were removed from the analysis. The remaining proteins were subjected to missing value imputation using the default parameters (width 0.3, down shift 1.8) of the Perseus imputation tool. Sex, age and post mortem intervals were compared between the three groups (control, early and late B/B stages) in each region using Chi-square test (for binary data) and linear regression (for continuous numerical values) to determine whether these variables differ between groups. These tests showed that the disease groups were unbalanced with respect to age (p-value < 0.0338) and sex (p-value < 0.1551) in the four brain regions (Fig. S1). Accordingly, all proteins significantly associated with age or sex (linear regression analysis, p-value < 0.05) were removed from the list of differentially expressed proteins. In order to evaluate differentially expressed proteins (DEPs) during disease progression, Student's *t*-test was applied to

compare early B/B (I-III) and late B/B (IV-VI) stages with the control group (p-value < 0.05, fold change ≤0.66 or ≥ 1.5) in each brain region. Analysis of DEPs between the 4 brain regions in health state was performed using one-way ANOVA with post-hoc Tukey's honestly significant difference (HSD) test. The following requirements were used to determine significance: adjusted p-value < 0.05 and fold change ≤0.66 or ≥ 1.5. Heat maps were generated from hierarchical clustering based on average Euclidean distance and complete linkage, using R.

Venn diagrams were generated with an online tool from Ghent University (http://bioinformatics.psb.ugent.be/webtools/Venn/). Protein-protein interaction networks were built with String version 10.5 (https://string-db.org/) using 0.7 as the minimum required interaction score (high confidence). Gene ontology enrichment analysis was carried out on String version 10.5 and DAVID version 6.8 (https://david.ncifcrf.gov/).

Verification of DEPs identified in the present work was performed by comparison with two other AD proteomic studies (Hondius et al., 2016; Seyfried et al., 2017), and only proteins reported to be significantly altered were used in the comparison. From the study reported in Seyfried et al., 2017, the results from dorsolateral prefrontal cortex were selected for verification, and proteins fulfilling the following criteria were considered as DEPs: ANOVA with post-hoc Tukey's HSD test p-value < 0.05. For the comparison, the highest log2 fold change values were used in case of all DEPs.

3. Results

3.1. Human brain proteome profiling

We employed a mass spectrometry-based approach to interrogate the human brain proteome during AD progression (B/B stages) in four distinct brain regions: entorhinal cortex (EC), parahippocampal cortex (PHC), temporal cortex (TC) and frontal cortex (FC). Importantly, we wanted to evaluate brain areas that are affected by tau pathology at different disease stages, in order to gain insights if there are common mechanisms or patterns shared between different brain regions during disease progression. Among the investigated regions EC and PHC that belong to the medial temporal lobe are affected already at the early, while the neocortical regions (TC, FC) are affected by tau pathology only at the late stages of AD (Braak and Braak, 1991). A total of 103 samples were analyzed individually, furthermore, digestion replicates were generated for each brain region in order to evaluate the reproducibility of sample preparation. As expected, the correlation was higher between digestion replicates than biological replicates from the same disease group (Fig. S2). In total 3809, 3815, 3610 and 3720 protein groups with at least 2 peptides were identified in EC, PHC, TC, and FC, respectively. There was a large overlap (> 85%) between the identified protein groups from different disease stages in each brain region as it is indicated in Fig. S3. Gene ontology enrichment for cellular components (GOCC) revealed similar categories for the four brain regions (Fig. S4).

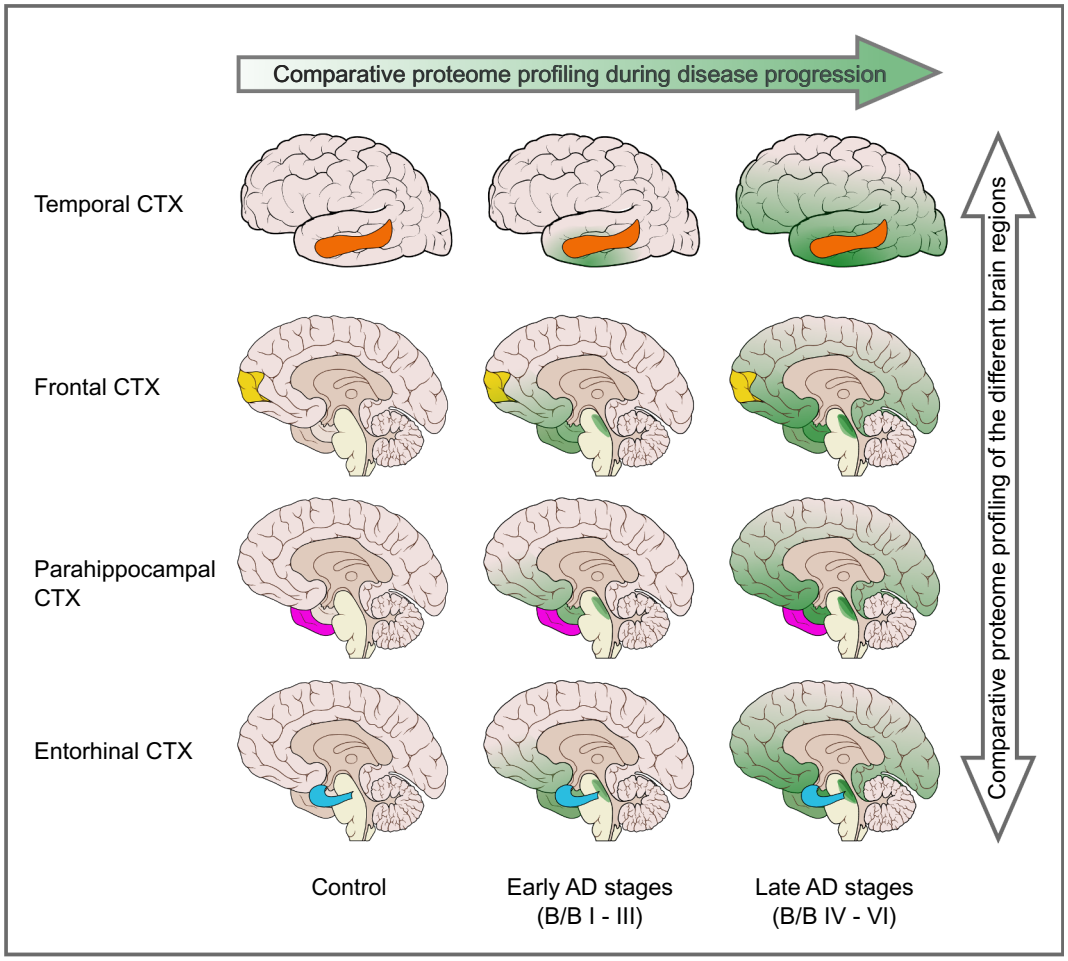

Fig. 1. Graphical illustration of the study design.
Two approaches were employed in the study: 1) comparative proteome profiling during disease progression to unravel altered proteins/pathways in different brain regions and 2) comparative proteome profiling of different brain regions in healthy subjects to investigate brain region vulnerability to AD.

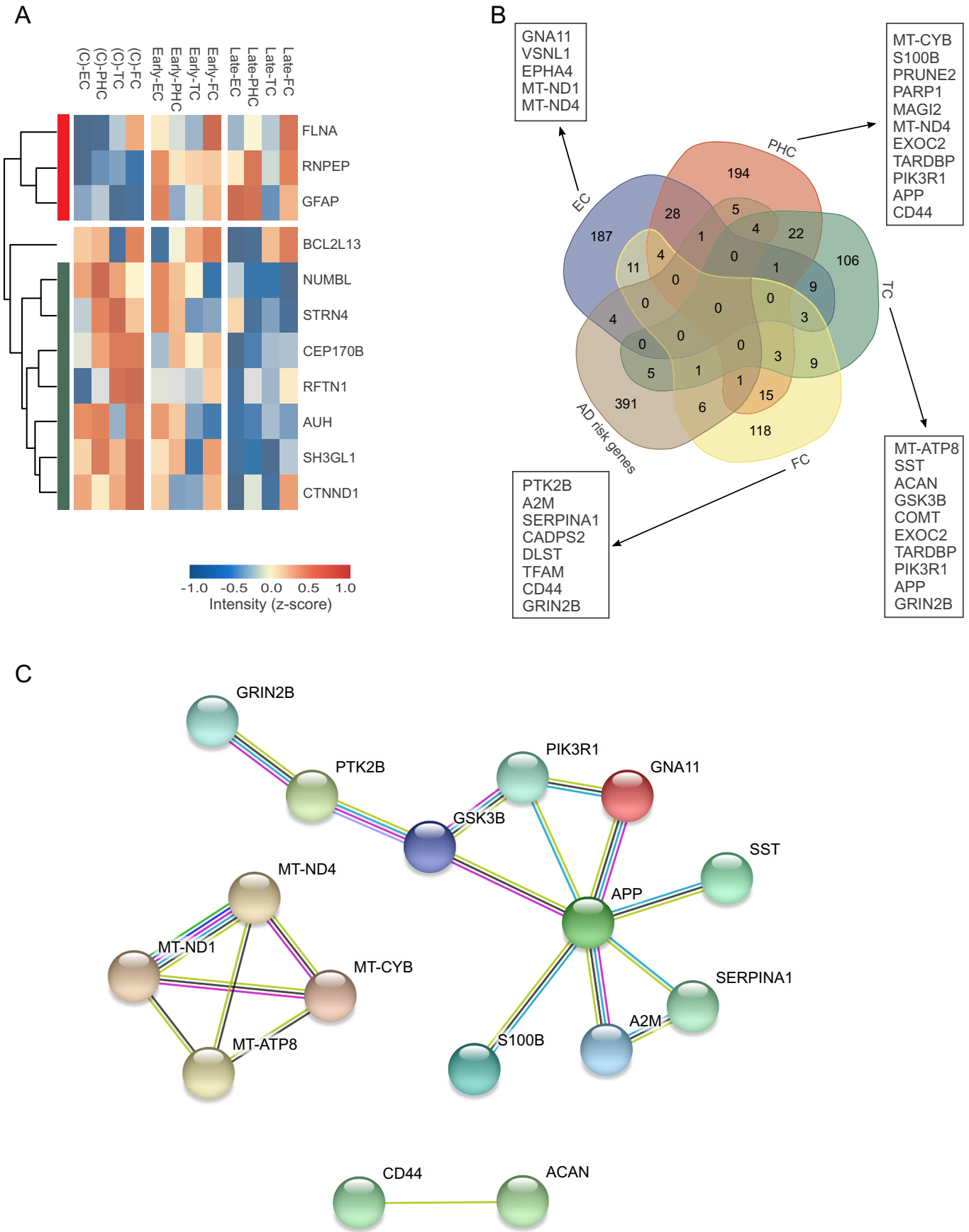

(caption on next page)

Fig. 2. Proteins differentially expressed during AD progression.
A) Hierarchical clustering of 11 proteins that are altered in 3 brain regions. Cluster in red: up-regulated proteins during AD course; Cluster in green: down-regulated proteins during AD course. B) Venn diagram showing the overlap of AD risk loci with DEPs found in each brain region. C) Protein interactome of DEPs described as AD risk genes. Line color indicates the type of interaction evidence (yellow: textmining, purple: experiments, light blue: databases, black: co-expression, blue: co-occurrence). (For interpretation of the references to color in this figure legend, the reader is referred to the web version of this article.)

3.2. Proteins differentially expressed during AD progression

In this work, we employed two approaches to analyze differences in proteome profiles of brain areas affected by tau in early (EC, PHC) and late disease stages (TC, FC) (Fig. 1). Firstly, in order to understand how the brain proteome is altered during AD progression, we investigated which proteins are differentially expressed when comparing early (B/B I-III) and late disease stages (B/B IV-VI) to control individuals in each brain region. Secondly, to investigate physiological proteomic signatures that might contribute to brain area susceptibility to AD, we compared the proteomic profiles of the four brain regions in healthy subjects (controls).

Regarding the first approach (investigation of changes in the proteome of each region during AD progression), a total of 248, 278, 163 and 171 proteins were significantly different in EC, PHC, TC, and FC, respectively, totalizing 737 proteins (Table S3). Interestingly, the highest numbers of DEPs were observed in the regions affected early by tau pathology. Early changes in protein levels were observed in each region but the number of altered proteins increased when the late disease stage was compared with controls (Fig. S5). The comparison of DEPs from various brain regions revealed that there is only a small overlap between regions, especially during the early stages, although there is an increase in the number of shared proteins during the late stages. The comparison of differentially expressed proteins found in each region indicated that in total 101 proteins are shared between two, and only 11 proteins are shared between three brain regions (Table 1, Fig. S6). Out of these 112 proteins, 99 showed similar expression level changes across brain regions (up- or down-regulated in all comparisons) and only 13 changed in opposite directions across comparisons (up-regulated in one and down-regulated in another brain region). Some of the aforementioned 11 proteins are involved in metabolic processes (CTNND1, FLNA, AUH, RNPEP, and NUMBL) and related to cell-adhesion: CTNND1, FLNA and NUMBL play a role in adherens junction organization; and CTNND1, FLNA and SH3GL1 are expressed in the cell junction. Hierarchical clustering of the 11 proteins altered in three brain regions was performed and a heat map was generated considering their expression during disease progression in all brain areas (Fig. 2A). Two main protein clusters were detached with opposite expression profiles during disease progression, in addition to Bcl-2-like protein 13 (BCL2L13) that was down-regulated in MTL but slightly up-regulated in the neocortex. The cluster with augmented expression levels in late disease stages consists of 3 proteins including two well-known AD players: filamin A (FLNA) and glial fibrillary acidic protein (GFAP), a marker of astrocytes, while the other cluster of 7 proteins shows reduced levels in AD compared to controls.

We wondered if some proteins that were found to be altered during disease progression have already been associated with genetic risk for AD. A comparison was done between all 737 differentially expressed proteins and a list of AD risk genes published recently (Hu et al., 2017). We found that 27 proteins have already been described as AD risk loci (Fig. 2B). With the aim to better clarify the relationship between these proteins, an interactome showing protein-protein interactions was built with String (Fig. 2C). The majority of proteins are connected, and APP appears as a central node with the highest number of interactions. Functional enrichment analysis revealed that synaptic proteins and proteins involved in oxidative phosphorylation are overrepresented. Additionally, some of these proteins are involved in pathways related to neurodegenerative disorders, such as Alzheimer's disease (APP, GRIN2B, GSK3β, MT-ATP8, MT-CYB), Parkinson's disease (MT-ATP8, MT-CYB, MT-ND1, MT-ND4) and Huntington's disease (GRIN2B, MT-ATP8, MT-CYB, TFAM).

3.3. Altered pathways during AD progression

In order to evaluate segregation of disease stages and to observe expression profiles, hierarchical clustering of DEPs from the four brain regions (EC, PHC, TC, and FC) was performed. Four major protein clusters were found, which represent distinct expression patterns (early-up, early-down, late-up and late-down) during disease progression. The majority of altered proteins were found down-regulated in AD considering all regions (> 70% in MTL and > 60% in the neocortex) (Figs. 3 and 4). With the aim to clarify which pathways and processes are altered during disease progression, each cluster was further subjected to enrichment analysis.

Regarding EC, pathway analysis revealed that the mitochondrial respiratory chain complex I assembly is significantly enriched in the early-down cluster that consists of 14 proteins, indicating an impairment in oxidative phosphorylation. The late-down cluster incorporates 189 proteins, among which proteins involved in vesicle-mediated and protein transport, translation including ribosome subunits, as well as synaptic proteins are highly enriched. A greater impairment in oxidative phosphorylation was also observed in this cluster. On the other hand, the early-up cluster presents 24 proteins, some of which are associated with cell-cell adhesion. 21 proteins belong to the late-up cluster, where cell adhesion and astrocyte development were found as enriched processes (Fig. 3 and Table S4).

Considering PHC, 104 proteins are present in the early-down cluster, and as it was seen in EC oxidative phosphorylation is significantly enriched. Actin filament and synapse-based processes are also present in this cluster. PHC late-down cluster is composed of 95 proteins, which are related to oxidative phosphorylation, translation, and synapse. Interestingly, these processes were also found in EC late-down cluster. PHC early-up cluster harbors 26 proteins, which are related to platelet aggregation and the regulation of cell shape. The late-up cluster has 39 proteins that are associated with extracellular matrix organization, cell adhesion and UDP-*N*-acetylglucosamine biosynthetic process (Fig. 3 and Table S4). Remarkably, proteins involved in cell adhesion were also present in EC early-up and late-up clusters.

Considering TC, the early-down cluster has 48 proteins that are mainly involved in synaptic processes and oxidative phosphorylation (respiratory electron transport chain). The late-down cluster presents 48 proteins that are related to cell adhesion and to the regulation of cytoskeleton organization. The early-up cluster consists of 62 proteins that are associated with the oxidation-reduction process, cholesterol metabolic processes and lipid transport. Only 5 proteins compose TC late-up cluster, where extracellular matrix organization is one of the few processes found enriched (Fig. 4 and Table S5).

Concerning FC, the early-down cluster contains 31 proteins, which are mainly synaptic proteins. In total, 61 proteins form the late-down cluster of FC, where synapse and protein translation were found enriched. FC early-up cluster presents 33 proteins, which are related to acute phase response and platelet activation. Finally, FC late-up cluster includes 26 proteins that are involved in extracellular matrix organization (Fig. 4 and Table S5).

Up and down-regulated proteins in each brain region were submitted to enrichment analysis for cellular component categories (GOCC) to unravel key cellular parts/organelles affected by the disease. This analysis revealed a remarkable down-regulation of the

Table 1
Differentially expressed protein (DEPs) during AD progression that are shared between brain regions represented by their log2 fold changes. Red color indicates up-regulated, blue color indicates down-regulated proteins in AD.

Gene name	Early B/B stages				Late B/B stages			
	EC	PHC	TC	FC	EC	PHC	TC	FC
GFAP	0.771			0.893	1.212	0.914		0.884
FLNA	1.286	0.911		1.369	0.949	1.008		
AUH				-0.834	-0.717	-0.684		
CEP170B					-1.123		-0.679	-0.636
CTNND1				-0.858	-1.568		-1.144	
BCL2L13			1.393		-2.675	-1.461	1.267	
RNPEP	1.153					0.845		0.837
RFTN1	0.652						-1.019	-0.842
SH3GL1						-0.836	-0.845	-0.840
STRN4						-0.879	-0.901	-0.665
NUMBL		-0.754				-1.446	-0.810	-0.991
CAPS		2.360			3.166	3.171		
ANXA1		1.475			1.801	1.964		
PLIN3					1.462	1.093		
BDH2					0.954	0.771		
RAB33B		-1.018			-0.606	-0.917		
MT-ND4					-0.632	-0.834		
RAP2A		-0.786			-0.647			
THY1					-0.681	-0.723		
RAB3GAP1					-0.683		-1.360	
GAP43					-0.751	-0.642		
FXYD7					-0.772	-1.828		
PCCB					-0.805	-0.700		
SYT7					-0.866	-0.868		
DIRAS2	-0.606				-0.886	-0.868		
HPCA					-0.901	-1.009		
PLXNA1				-1.301	-0.908			-1.369
RPTOR				-1.864	-0.949			
ESYT1					-0.972		0.675	
MARK2			-0.911		-0.995		-0.830	
GMPS					-1.021	-1.262		
LRRC57	-0.638				-1.058	-0.708		
RPS13					-1.135	-1.341		
SRC		-1.167			-1.192			
SCN2A					-1.210			-0.590
EMC1	-0.879				-1.238			-0.812
FGF12		-0.927			-1.249	-0.614		
ATPAF1	-1.188				-1.281	-1.472		
UQCR10					-1.326	-0.607		
DIRAS1					-1.372		1.171	
VAMP2					-1.377	-0.684		
C2CD4C					-1.412			-1.571
GGA3					-1.412			1.016
SLC25A46					-1.414	-2.197		
AP3M2					-1.590	-1.647		
RAB10				-1.141	-1.684			
CA4				-0.755	-1.770			-1.141
IGSF21					-1.781			-0.812
SCYL1			-2.280		-2.437			
KYAT3	1.405	0.862						
RPA3	1.370			-0.858				
GNG5	1.103		2.394					
CLIC1	0.948					1.083		
CAPG	0.826			0.761				
GYG1	0.685						0.628	

(*continued on next page*)

Table 1 (*continued*)

DYNLL2	-0.630	-0.688				-1.149		
SDHC	-0.711					-1.596		
TRIM3	-1.060		-0.652					
CHN1	-1.301		-0.794					
EXOC7	-1.905	-2.113				-2.009		
DLGAP1			-1.136			-0.705		
ERC2						-1.588	-1.146	
PFDN6				-1.484		-1.377		
VGF						-1.890		-2.014
EXOC3				-0.778		-1.339		
PFKFB2				0.991		1.122		
ORM1				1.286			0.883	1.590
ALB						0.709		0.604
APP						1.447	0.843	
CD63		-1.245				-0.683		-0.608
MAP2			-0.926			-0.799	-0.586	
VCAN						0.847		0.805
ACYP2			-0.727			-0.795		
COX6B1			-1.084			-0.808		
GABRA1						-0.907	0.980	
CD44						2.354		1.362
RAB3B							-0.888	-1.126
GART				0.619		1.012		
FDXR			1.477			-1.182		
PIK3R1						-0.932	-0.775	
CORO1A						-0.614	-0.666	
SPR		0.687					0.984	
KRT2			2.237			-2.021		
AGFG1						-0.743	-0.630	
SUB1				-1.585		-1.767		
RPL23A			-1.088					-0.867
RPL23						-0.952	1.094	
FKBP1A						-0.859	-0.890	
GRIN1						-1.196		-1.017
TARDBP			-0.582			0.818		
GRIN2B							-1.443	-0.708
SCARB2			1.447			1.128	1.473	
CTTN			-0.858			-1.159		
CAMK4							-0.587	-0.625
KIAA1217						-1.347		-1.567
SLC27A4				-0.761		-0.946		
SH2D5			-1.312				-1.177	-1.097
RIMS1				-0.738		-0.842		-0.863
HOMER1						-0.852	-0.668	
DMXL2						-0.856		-0.693
SCFD1			-0.621				-0.905	0.711
NRGN			-1.056			-0.820	-1.152	
ACSF2						-1.048		-1.014
EXOC2						-0.599	0.846	
SYNGAP1						-0.642	-0.618	
SGIP1							-1.015	-0.628
RAB11FIP5		-1.105	-1.037			-1.640		
PHACTR1						-0.969	-0.956	
HAPLN2						0.754	1.112	
TANC2				-0.626			-0.888	
BSN							-0.669	-0.814
PCLO			-1.604			-0.788		

mitochondrial and ribosomal proteins in MTL regions. In addition, a global down-regulation of synaptic, dendritic and axonal proteins occurred in all 4 regions (Fig. 5A). Mitochondrial oxidative phosphorylation impairment and translation dysregulation were evident primarily in the two MTL regions, however, a few related proteins were found altered in the neocortex as well (Table S4 and Table S5). Proteins associated with oxidative phosphorylation and translation predominantly show a decreasing expression profile in MTL during disease progression. On the contrary, in neocortex the majority of these proteins are unaffected, and only a few proteins were found significantly down-regulated in AD (Figs. 5B and C).

3.4. Proteome profiling of healthy subjects in different brain regions

Currently, the matter of brain area vulnerability in neurodegenerative disorders is a highly debated and unsolved question. Our goal was to identify distinctive proteomic signatures in the brain that can be associated with the susceptibility of some areas to present early degeneration in AD. The comparison of the proteome from healthy individuals (controls) resulted in 648 differentially expressed proteins between the four brain areas (Table S6). Hierarchical clustering of all 648 DEPs was performed and the resulting dendrogram clearly separated MTL samples from neocortical samples (Fig. 6A). DEPs were divided into 2 major clusters: one group of 238 proteins with higher levels in the neocortex compared to MTL (MTL-down) and another group of 410 proteins that are more expressed in MTL (MTL-up).

In order to clarify which pathways are more active in specific brain areas, each cluster was subjected to enrichment analysis using DAVID (Table S7). It is noteworthy that several overrepresented pathways in the MTL-up cluster have already known link to AD, such as energy production (oxidative phosphorylation), protein translation, proteasome (Fig. 6B). Long-term potentiation is also significantly enriched in this cluster. A total of 16 ribosomal proteins (RPL17, RPL27A, RPL36, RPL38, RPS4X, RPS16, RPL23, RPL9, RPS14, RPS12, RPL10, RPL5, RPS10, RPS20, RPS11, RPL4) and 10 proteins from proteasome-complex (PSMA2, PSMD12, PSMC4, PSME1, PSMC2, PSMB3, PSMC1, PSMB2, PSMD7, PSMD8) were found among the proteins significantly upregulated in MTL. Additionally, a greater number of mitochondrial proteins was recognized in cluster MTL-up (79 proteins, 19.27%) compared to cluster MTL-down (24 proteins, 10.08%).

Regarding the cluster of proteins significantly up-regulated in the neocortex, some proteins involved in proteasome regulation (negative regulation of proteasomal ubiquitin-dependent protein catabolic process (GO:0032435)), e.g. UBXN1, BAG6 and CCAR2 are enriched in this cluster, but none of them belongs to the proteasome complex. Proteins involved in mRNA splicing via spliceosome (HNRNPL, SRSF1, NONO, SF3B1, SRSF7, ELAVL1, RBMX, YBX1) and in integrin-mediated signaling pathway (ADAM23, LAMA5, SEMA7A, ADAM22, ZYX, DST) are exclusively enriched in this cluster. Cytoskeleton and synapse-related proteins are overrepresented in both clusters (Table S7).

We further investigated whether some of these proteins that differentiate MTL and neocortex in healthy tissue were altered in AD as well. Interestingly, 226 proteins (out of 648) showed altered levels during disease progression. We found that proteins with higher expression level in MTL were almost exclusively down-regulated in the same brain region during AD progression, and similar behavior was observed in the neocortex, i.e. many proteins with higher abundance in healthy neocortical tissue showed reduced expression in this brain region during disease.

3.5. Comparative analysis with other proteomic studies in AD

With the aim to confirm the validity of our findings, we sought to compare our full dataset of dysregulated proteins during AD progression (737 proteins in the four brain regions) with the lists of altered proteins reported by two recently published AD proteomic studies (Hondius et al., 2016; Seyfried et al., 2017). In total, 275 proteins were shared between at least two studies, and 24 proteins were dysregulated in AD in all three studies (Fig. 7A; Table S8). The common proteins showed similar behavior in all proteomic studies, 19 proteins (G3BP2, ABI2, ACTR3B, TWF2, SV2B, SYNGAP1, ANKS1B, CORO1A, HPCA, PCDH1, CAMK2A, ACTN2, TUBB3, PACSIN1, NCKAP1, SLC8A2, FAM162A, GNAZ, GDAP1) were found down-regulated, while 5 (TLN1, VIM, G6PD, GFAP, PLCD1) were up-regulated in AD. (Table S8, highlighted). This is especially interesting since the previous works focused on different brain regions, e.G. *hippocampus* (Hondius et al., 2016) and dorsolateral prefrontal cortex (Seyfried et al., 2017).

To unravel the role of the conserved proteins, functional enrichment analysis was carried out using proteins shared between at least two studies. Only concordant proteins (changes in their expression levels show the same direction in all studies) were evaluated in this analysis. Among up-regulated proteins, the most significant biological process categories were extracellular matrix organization, cell adhesion, lipid metabolic processes, platelet degranulation and astrocyte development (Fig. 7B). On the other hand, down-regulated proteins are mainly involved in microtubule-based processes, vesicle-mediated transport, and synaptic vesicle endocytosis, ephrin receptor signaling, and cytoskeleton organization (Fig. 7B).

Remarkably, 195 proteins that showed alteration during AD in the present study have already been described previously. Additionally, the majority of these proteins (166) shows similar expression level changes to what previously reported (Table S8). With the aim to better assess the similarity between our results and other proteomic studies, we compared the log2 fold changes of overlapping altered proteins (Fig. 7C). Moderate correlation (R^2) was found between our results and the datasets from Hondius et al. and Seyfried et al. that comprised brain regions similar to those investigated in the current study. It is important to note that, although there are differences between the log2 fold changes of various proteins, which has an impact on the correlation, the great majority of common proteins show accordant changes across the studies. Overall, these results reinforce the validity of our proteomic findings.

3.6. Verification of a set of differentially expressed proteins by targeted MS/MS

To confirm the validity of our label-free quantification approach a set of differentially expressed proteins from the discovery phase were selected for PRM analysis. 75 peptides corresponding to 21 proteins were included and successfully detected in the final PRM assay panel. By comparing controls with the AD groups 16 proteins out of the 17 DEPs showed significant differences in at least one brain region, furthermore, expression level alterations between the MTL and neocortical regions were confirmed for 5 proteins including APOE (Table S9, Fig. 8A and B). In addition to determining APOE level with the help of the isoform-specific SIS peptides we were able to identify APOE phenotypes as well, as we described it in our previous publication (Rezeli et al., 2015). We found all six different phenotypes among the samples, but we couldn't make a systematic quantitative comparison between phenotypes since > 70% of the samples were ε3 homozygotes (Table S1).

In contrast to the discovery phase during PRM analysis Aβ level was measured separately from APP by using a peptide (LVFFAEDVGSNK), corresponding to residues 17–28 of Aβ. Although this peptide is not suitable for differentiating between the holoprotein and its fragment, the different behavior of the Aβ peptide and the other APP peptides indicates that it is appropriate for measuring Aβ levels. Significant increase in the Aβ level was observed in each region during AD progression, while APP was constant or slightly decreased (Fig. 8C).

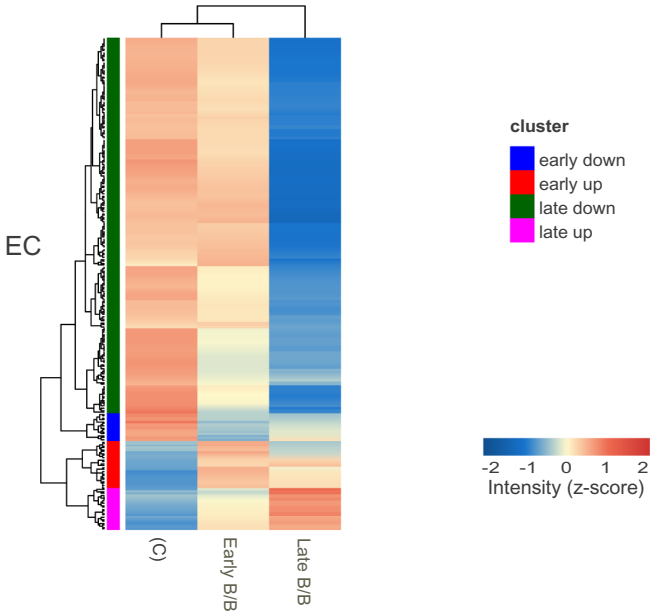

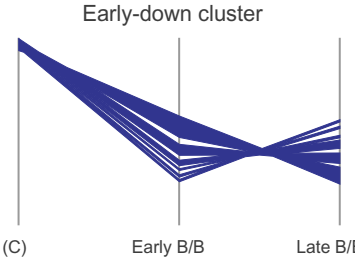

Area	GOBP Term	P-Value
EC	lipid homeostasis	2.98E-02
EC	mitochondrial respiratory chain complex I assembly	4.77E-02
PHC	glutamate secretion	5.19E-04
PHC	pos.reg. of prot. insertion into mitochondrial membrane	6.38E-04
PHC	calcium ion-regulated exocytosis of neurotransmitter	1.38E-03
PHC	actin cytoskeleton reorganization	2.38E-03
PHC	vesicle fusion	4.54E-03

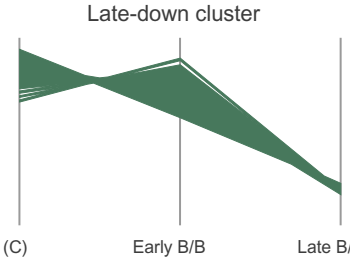

Area	GOBP Term	P-Value
EC	vesicle-mediated transport	4.38E-06
EC	intracellular protein transport	3.80E-05
EC	nuclear-transcribed mRNA catabolic process	2.49E-04
EC	protein localization to plasma membrane	5.01E-04
EC	translational initiation	5.85E-04
PHC	SRP-dependent cotranslational membrane targeting	1.26E-03
PHC	oxidative phosphorylation	1.86E-03
PHC	nuclear-transcribed mRNA catabolic process	2.99E-03
PHC	mitochondrial respiratory chain complex I assembly	3.86E-03
PHC	translational initiation	4.94E-03

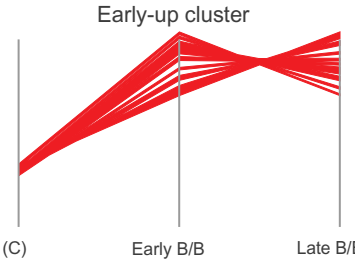

Area	GOBP Term	P-Value
EC	reg. of cellular response to heat	4.29E-03
EC	cell-cell adhesion	5.10E-03
EC	autophagosome maturation	3.23E-02
PHC	platelet aggregation	2.31E-05
PHC	reg. of cell shape	8.89E-04
PHC	3'-UTR-mediated mRNA stabilization	2.30E-02

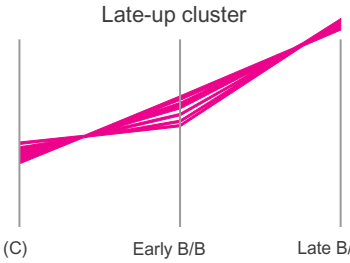

Area	GOBP Term	P-Value
EC	pos.reg. of vesicle fusion	7.90E-03
EC	Bergmann glial cell differentiation	1.01E-02
EC	intermediate filament organization	1.80E-02
EC	astrocyte development	1.80E-02
EC	cell-cell adhesion	3.70E-02
PHC	UDP-N-acetylglucosamine biosynthetic process	2.43E-04
PHC	extracellular matrix organization	7.92E-04
PHC	N-acetylneuraminate catabolic process	1.28E-02
PHC	cell-cell adhesion	2.01E-02
PHC	carbohydrate phosphorylation	4.82E-02

Fig. 3. Hierarchical clustering and functional enrichment analysis of DEPs in the MTL during AD progression.
Heat maps built with DEPs found in EC and PHC. Clusters representing the four typical expression profiles are colored accordingly to the heat maps. The 5 most significant biological processes (GOBP) are listed for each expression profile.

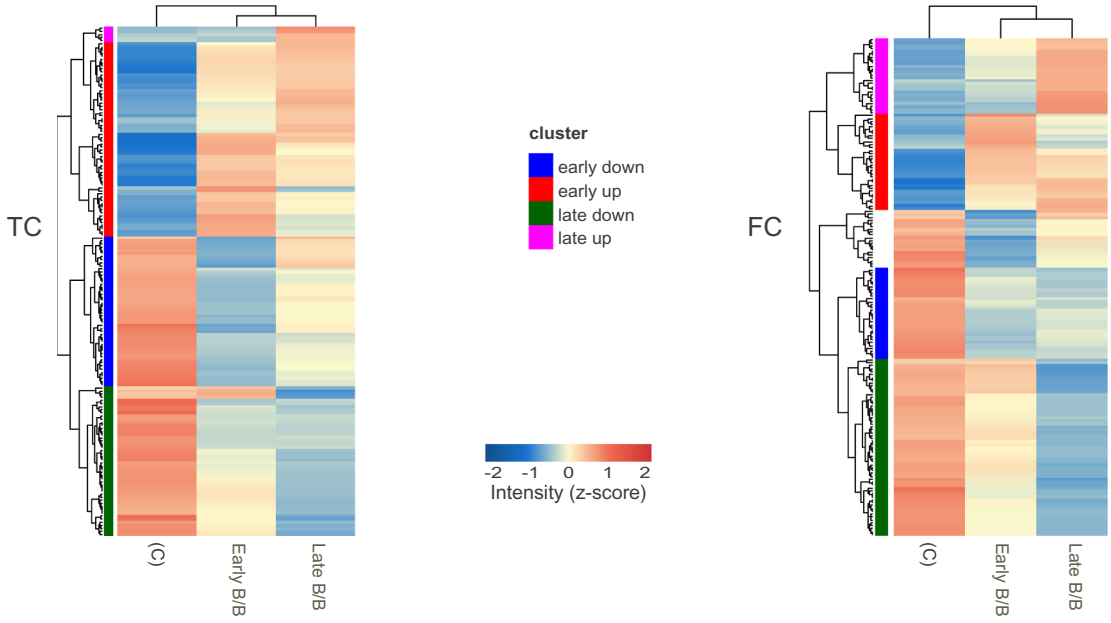

Area	GOBP Term	P-Value
TC	MAPK cascade	4.07E-03
TC	synapse assembly	1.02E-02
TC	chemical synaptic transmission	2.20E-02
TC	dendritic spine morphogenesis	2.96E-02
TC	respiratory electron transport chain	4.89E-02
FC	synaptic vesicle exocytosis	6.07E-04
FC	neurotransmitter secretion	3.25E-03
FC	chemical synaptic transmission	7.26E-03
FC	cell migration	3.31E-02
FC	Wnt signaling pathway	3.86E-02

Area	GOBP Term	P-Value
TC	cell-cell adhesion	7.05E-05
TC	intracellular signal transduction	3.91E-03
TC	adherens junction organization	4.22E-03
TC	actin cytoskeleton reorganization	6.73E-03
TC	movement of cell or subcellular component	2.13E-02
FC	SRP-dependent cotranslational membrane targeting	3.08E-03
FC	long-term memory	3.38E-03
FC	nuclear-transcribed mRNA catabolic process	5.96E-03
FC	chemical synaptic transmission	6.44E-03
FC	translational initiation	8.77E-03

Area	GOBP Term	P-Value
TC	oxidation-reduction process	1.16E-03
TC	intracellular sequestering of iron ion	2.13E-02
TC	cholesterol metabolic process	2.46E-02
TC	methylation	2.81E-02
TC	lipid transport	3.02E-02
FC	blood coagulation, fibrin clot formation	2.51E-08
FC	platelet degranulation	3.66E-08
FC	pos.reg. of adhesion-dependent cell spreading	3.00E-05
FC	acute-phase response	5.48E-05
FC	platelet aggregation	6.38E-05

Area	GOBP Term	P-Value
TC	extracellular matrix organization	4.59E-02
FC	bicarbonate transport	1.64E-03
FC	neurofilament bundle assembly	4.10E-03
FC	axon development	1.36E-02
FC	extracellular matrix organization	2.92E-02
FC	cellular response to fibroblast growth factor stimulus	4.03E-02

Fig. 4. Hierarchical clustering and functional enrichment analysis of DEPs in the neocortex during AD progression.
Heat maps built with DEPs found in TC and FC. Clusters representing the four typical expression profiles are colored accordingly to the heat maps. The 5 most significant biological processes (GOBP) are listed for each expression profile.

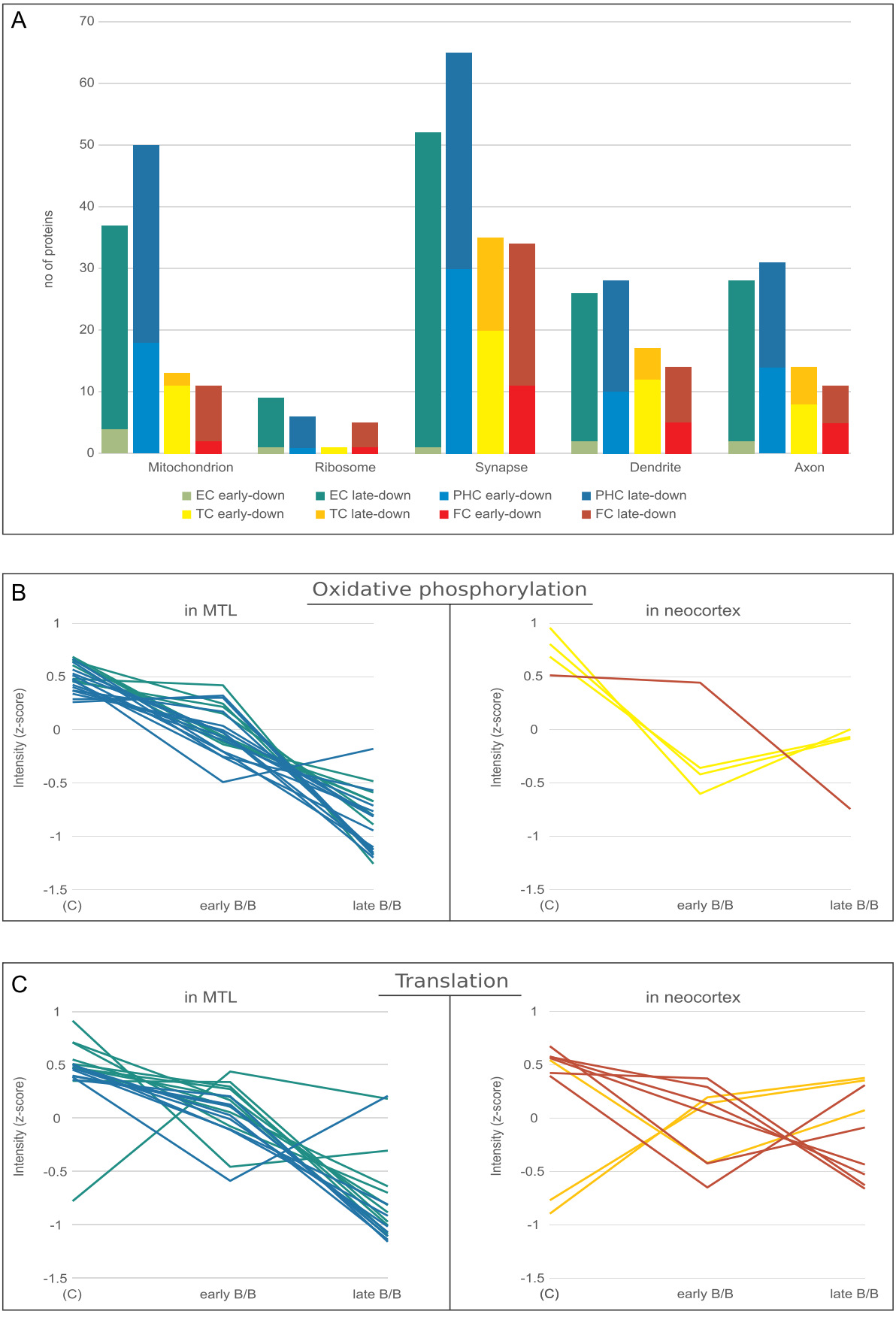

Fig. 5. Key cellular parts/organelles and pathways affected by AD.
A) Representative cellular component categories (GOCC) in down-regulated protein clusters. B) Expression profiles of proteins related to oxidative phosphorylation. C) Expression profiles of proteins involved in translation.

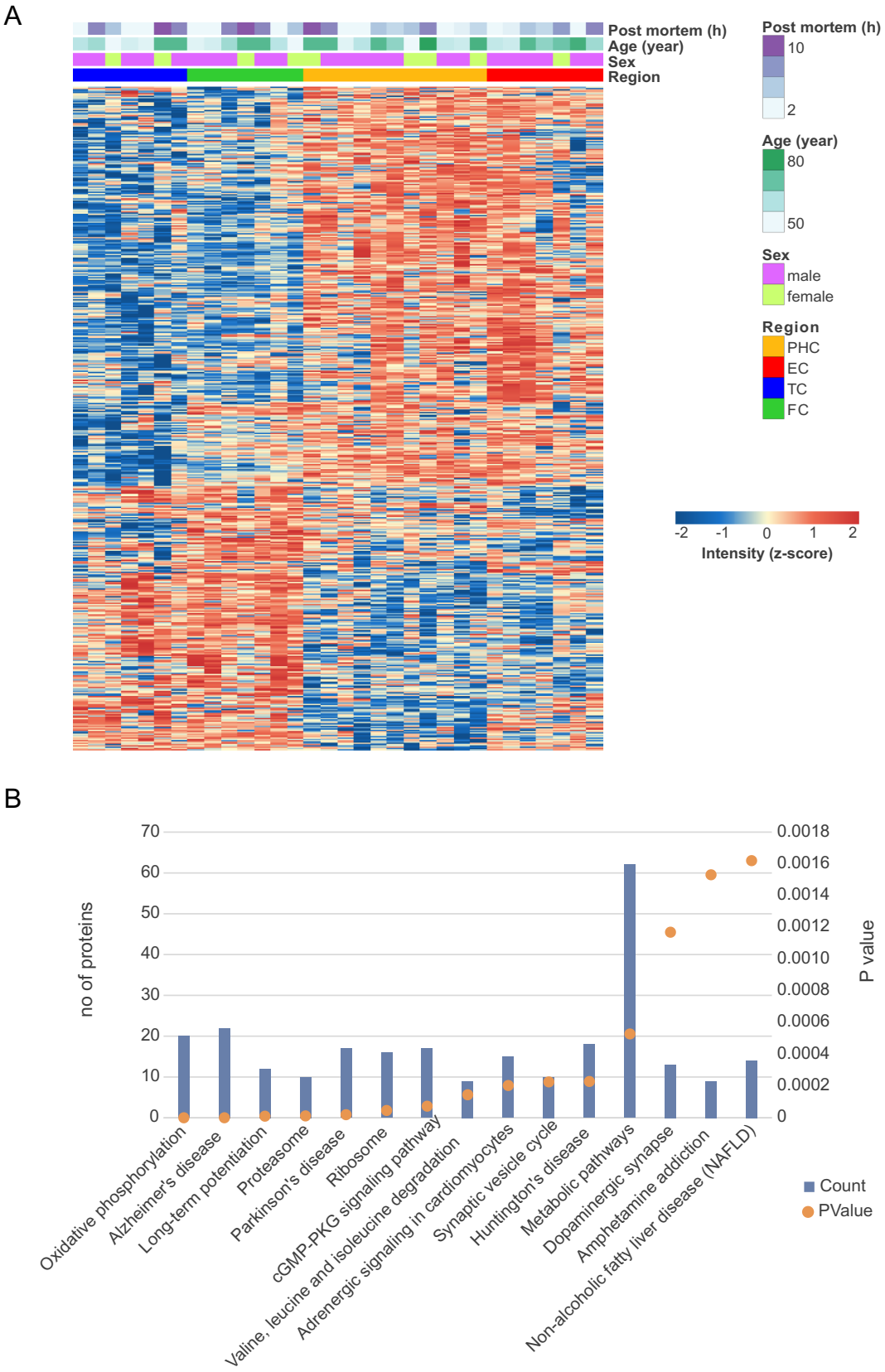

Fig. 6. Hierarchical clustering and KEGG pathway analysis of DEPs between brain regions in healthy subjects.
A) Heat map built with DEPs between brain regions. B) Top 15 KEGG pathways enriched for proteins up-regulated in MTL.

A

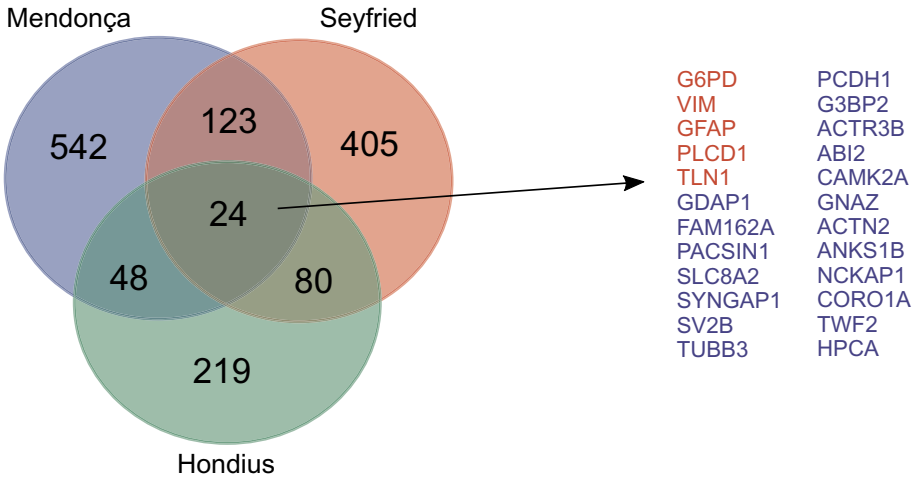

B

GOBP (up-regulated in AD)	Count	PValue
extracellular matrix organization	8	1.20E-05
cell-cell adhesion	8	9.10E-05
platelet aggregation	4	5.60E-04
intermediate filament organization	3	1.80E-03
astrocyte development	3	1.80E-03
lipid metabolic process	5	3.40E-03
platelet degranulation	4	7.80E-03
osteoblast differentiation	4	8.00E-03
cell adhesion	7	9.20E-03
substantia nigra development	3	1.60E-02
axo-dendritic transport	2	2.00E-02
dopamine catabolic process	2	2.00E-02

GOBP (down-regulated in AD)	Count	PValue
microtubule-based process	7	9.00E-07
ephrin receptor signaling pathway	9	1.30E-06
cytoskeleton organization	11	2.60E-06
synaptic vesicle endocytosis	5	1.20E-05
regulation of cardiac conduction	7	1.30E-05
Rac protein signal transduction	5	2.50E-05
pos. reg. of Arp2/3 complex-mediated actin nucleation	4	2.70E-05
clathrin-mediated endocytosis	5	3.10E-05
intracellular protein transport	11	7.30E-05
vesicle-mediated transport	9	8.80E-05
glutamate secretion	5	1.20E-04
regulation of synaptic plasticity	5	2.10E-04

C

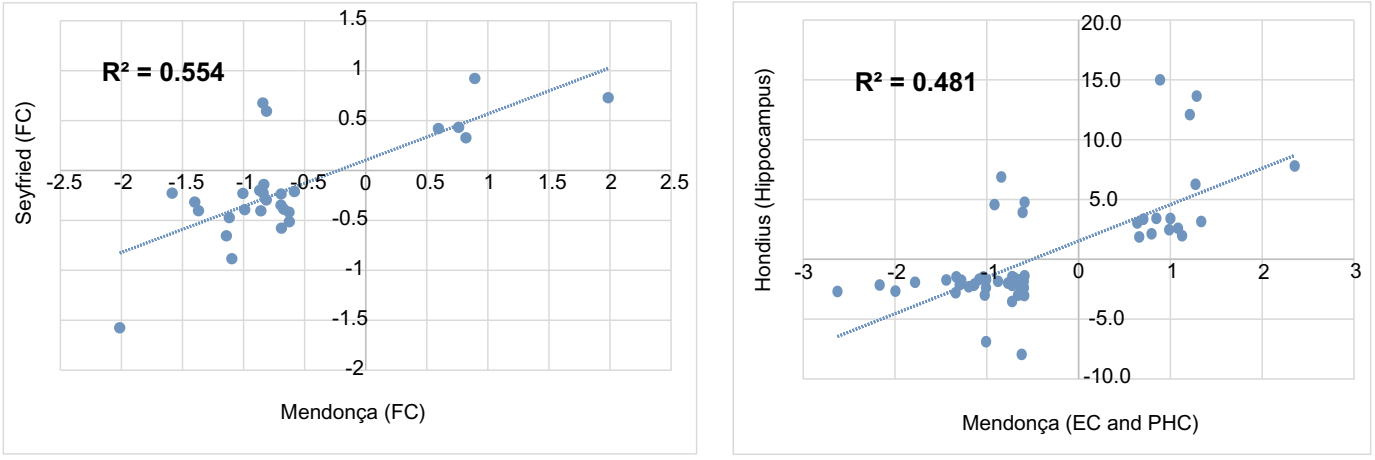

Fig. 7. Comparison of the altered proteins with independent AD proteomic datasets.
A) Venn diagram showing the overlap of DEPs between the present work and two other proteomic studies. B) Gene ontology (GOBP) enrichment analysis for overlapping proteins between at least two proteomic datasets (n = 275). C) Log2 fold changes of shared proteins between the current work and two other proteomic studies; the general correlation is shown (R^2).

4. Discussion

4.1. Proteomic changes during AD progression show a complex scenario with a few shared but mostly specific processes in the different brain regions

We observed 112 dysregulated proteins and a few pathways during AD course that are shared between 2 or more brain regions, possibly indicating their importance in the pathogenesis of the disease. Strikingly, the great majority of these proteins shows concordant changes in their expression levels in AD, further reinforcing the existence of common key processes in distinct brain regions (Table 1). Many proteins, however, were exclusively dysregulated in specific brain areas and the majority of altered pathways during the disease course was specific to certain brain regions. Regarding the progress of the disease, the similarities and differences found between the individual brain regions are most likely linked to the high degree of specialization of the brain. In accordance with the endogenous specificities of various brain areas, we hypothesize that genetic and environmental triggers of AD affect individual brain regions differentially, and this is reflected in the found diversity of dysregulated protein expression. In other words, we assume that the regionally different responses to early AD triggers are the consequences of the different

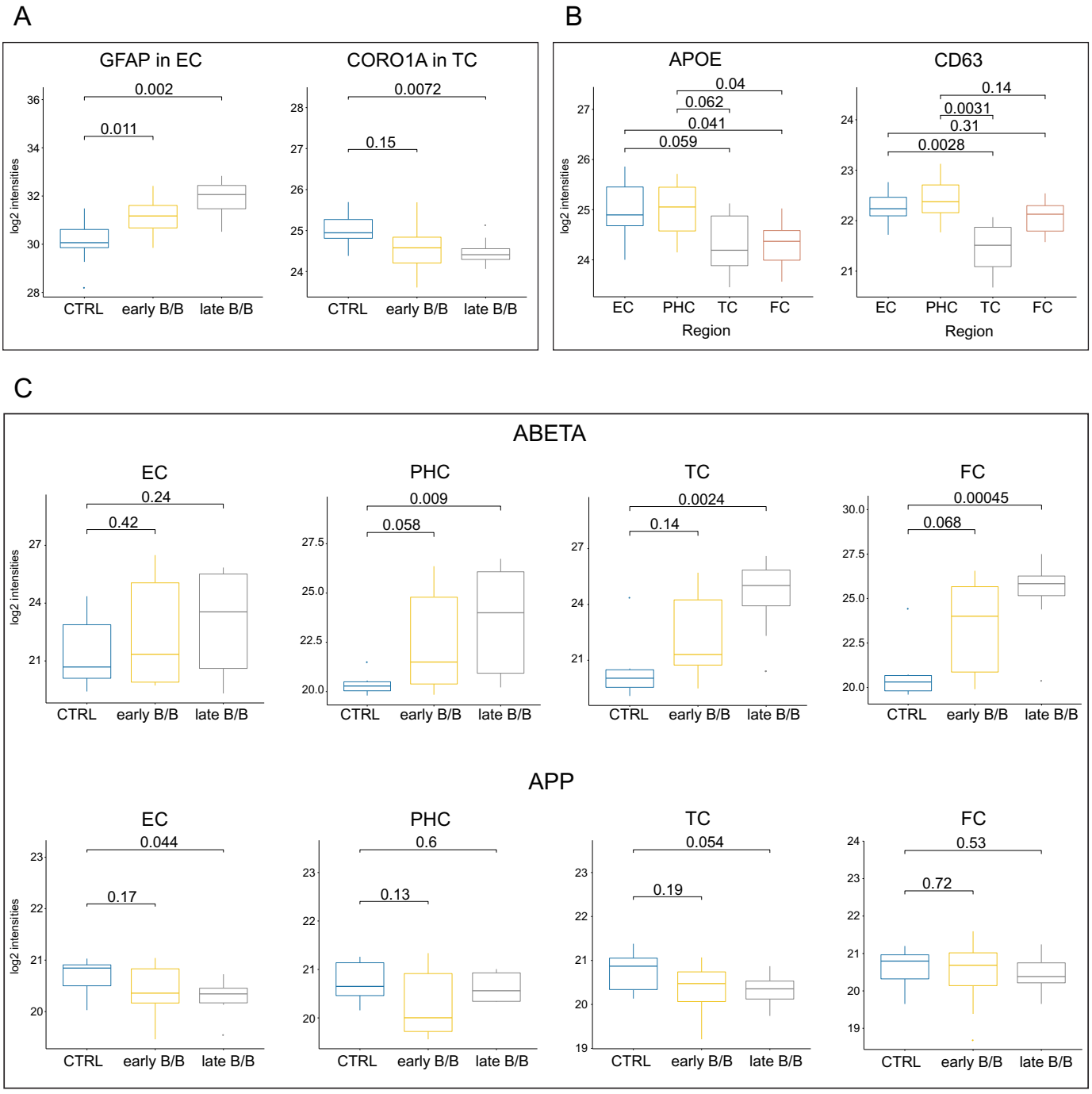

Fig. 8. Verification of a set of differentially expressed proteins by PRM.
A) Box-plot representing GFAP and CORO1A expression levels in EC and TC, respectively. B) Box-plot representing total APOE and CD63 expression levels of control subjects in 4 different brain regions. C) Box-plot representing ABETA and APP expressions in 4 different brain regions during AD progression.

proteomic background of each region. In some regions, proteomic changes may already be observed independent of the presence of classic pathological features of AD (e.g. tau protein aggregation). For instance, changes of the proteome in neocortical areas were observed in early B/B stages, suggesting that these regions have already responded to AD triggers regardless of tau seeding. According to our proteomic data synapse loss occurred in all analyzed regions, indicating that this process is ubiquitous in AD.

4.2. Synapse loss, translation dysregulation, and oxidative phosphorylation impairment during AD progression and their implications to disease

Processes associated with synapse were found down-regulated in AD in all four brain areas (Fig. 5A). Synapse loss is a pathological hallmark of AD and it is an early event in disease, occurring before neuron death (Scheff et al., 2006). Synaptic degeneration presents the best correlation with cognitive impairment, even higher than NFT or Aβ plaques deposition (Terry et al., 1991). The alteration of synaptic proteins was observed in both neocortical regions during early B/B stages (Table S5), which suggests that earlier events, occurring before the accumulation of insoluble tau tangles, trigger neuron dysfunction. This is supported by previous studies, which reported that synapse loss occurs before tangles formation in a tauopathy mouse model (Yoshiyama et al., 2007) and soluble tau causes synaptic dysfunction in an early AD model (Polydoro et al., 2013). Additionally, Aβ peptide has also been shown to cause synaptic degeneration (Walsh et al., 2002).

Several proteins involved in translation were found down-regulated in AD, mostly in 3 regions (EC, PHC, and FC). In total, 18 ribosomal subunits and 4 translation initiation factors showed reduced levels in these regions, however, in TC, only 3 proteins associated with translation were altered (1 down- and 2 up-regulated in AD) (Table S10). Some of the translation regulators were altered already in early B/B stages in neocortical regions, indicating dysregulated pathways before insoluble tau deposition. In line with our findings, several studies reported altered protein synthesis and ribosomal protein expression in various brain regions from AD patients (Ding, 2005; Garcia-Esparcia et al., 2017; Hernández-Ortega et al., 2015). Previous research identified a high number of translation machinery members among Aβ oligomers interacting partners (Virok et al., 2011), and it was found that tau interactome is enriched for proteins involved in translation and RNA processing (Gunawardana et al., 2015). Furthermore, it was reported that tau isolated from AD patients binds to more ribosomal proteins than tau from control subjects, and tau oligomers inhibit translation process (Meier et al., 2016). Table S10 summarizes the 24 dysregulated translation proteins in our AD cohort, associating our findings with literature data.

Reduced levels of proteins associated to oxidative phosphorylation were observed during early B/B stages in both MTL regions, with a higher number of proteins being affected during late stages (Fig. 5B, Table S4). In both EC and PHC, subunits of all electron transport chain complexes (I-V) were down-regulated. Additionally, several mitochondrial proteins were down-regulated in the two MTL regions (Fig. 5A). In contrast, in neocortical regions, only 4 proteins linked to oxidative phosphorylation were down-regulated (NDUFS6, COX6B1, and MT-ATP8 in TC, and NDUFA6 in FC). Hypometabolism is a known feature of AD brains, occurring years before the onset of symptoms in AD-vulnerable regions (de Leon et al., 2001; Mosconi et al., 2008). Previous studies with human tissue and animal models showed that proteins involved in energy generation in mitochondria, including mitochondrial electron transport chain subunits, are dysregulated in AD (Liang et al., 2008; Shevchenko et al., 2012). Finally, a complex regulatory mechanism underlies metabolism control, Aβ, and tau. Aβ and tau have been implicated in the impairment of oxidative phosphorylation (Rhein et al., 2009) and it was reported that APP is able to inhibit oxidative phosphorylation independently of Aβ peptide (Lopez Sanchez et al., 2017). Animal studies have demonstrated that tau has a new physiological function in insulin signaling regulation (Marciniak et al., 2017) and that energy deprivation increases the translation of BACE1, resulting in higher Aβ levels (O'Connor et al., 2008). Furthermore that glucose deficit induces tau phosphorylation and aggregation in a tauopathy mouse model (Lauretti et al., 2017).

4.3. Relationships of AD-related differentially expressed proteins to other diseases

Because it is rather difficult to find non-demented elderly controls without tau pathology, our groups were not fully balanced with respect to age. To overcome this issue, we removed all proteins significantly associated with age from the list of differentially expressed proteins. Investigating the set of age-associated proteins we found that our findings were consistent with a previous report (McKetney et al., 2019), as a little overlap was presented between regions, and a large proportion of these age-related proteins was associated with extracellular exosome (p-value = 6.2e-86) and membrane (p-value = 8.9e-29).

Furthermore, in order to examine what diseases could be related to the proteins differentially expressed between AD and controls (DEPs), Ingenuity analysis was performed. It allowed elucidating disease annotations significantly overrepresented among the DEP sets (Fig. S7). Interestingly, in very few cases the same disease annotations were overrepresented among DEPs for different brain regions (e.g. Seizures). Notably, for late disease stages and the FC region, overrepresented diseases included cancer, cardiovascular disease, and neurological disorders (e.g. epilepsy, brain neurodegeneration). For late B/B stages and the PHC region, most of the overrepresented disease annotations related to neuropsychiatric disorders (e.g. epilepsy, neuromuscular disease, schizophrenia), while in the TC region, inflammatory diseases were noteworthy. The sets of DEPs for early B/B stages were much smaller than those for late stages, consequently, fewer disease annotations were overrepresented (Table S11). Among these, pervasive developmental disorder (EC region) stood out.

The complex relationship between AD and other diseases is far from being fully understood as can be exemplified by the 86 differentially expressed proteins related also to melanoma according to the Ingenuity database (Fig. S8). This protein set includes both down- and upregulated proteins from various subcellular compartments, among them regulators such as CUL1 and CD44.

4.4. The vulnerability of brain areas to AD

An intriguing question in AD and other neurodegenerative disorders is why do some brain regions accumulate toxic protein aggregates and degenerate first. To gain potential insights into this, we analyzed proteomic differences between EC, PHC, TC, and FC in healthy control subjects.

Hierarchical clustering resulted in clear segregation of MTL and neocortical samples (Fig. 6A) that is consistent with the anatomical and functional differences of these regions. The MTL is involved primarily in memory functions (Squire et al., 2004), while the neocortex is rather related to cognitive processes (Rakic, 2009). MTL has high energy demands due to increased synaptic plasticity (memory formation and storage) and the presence of large neurons (Mosconi, 2013), which is in line with our results that metabolism-related pathways (metabolic pathways, oxidative phosphorylation, insulin signaling) and mitochondrial proteins were highly overrepresented in the cluster of proteins with augmented levels in MTL. Translation and proteasome pathways were also significantly enriched in MTL, indicating an accelerated proteostasis; as well as long-term potentiation that is consistent with EC and PHC involvement in memory formation (Fig. 6B). Interestingly, Alzheimer's disease KEGG pathway was also found enriched in the cluster of proteins overexpressed in MTL (22 proteins, p-value = 1.61e-7).

Remarkably, one of these AD proteins was APOE, the major genetic

risk factor for late-onset AD (Corder et al., 1993). We found that APOE level is generally higher in MTL compared to the neocortex, however, statistically significant differences were observed only between PHC and TC in the discovery dataset, as well as between both MTL regions and FC in the PRM dataset (Table S6, Fig. 8B). A previous work reporting that APOE mRNA level is augmented in EC compared to other brain areas (Liang et al., 2007) also strengthens our assumption that the MTL expresses APOE in higher level. Nevertheless, further studies are required to confirm the link between increased APOE level and AD vulnerability.

Recent studies elucidated the missing link between APOE, Aβ and tau, since it has been shown that *APOE* ε4 allele mediates and exacerbates tau toxic effects (Shi et al., 2017) and APOE mediates APP transcriptional regulation in such a way that *APOE* ε4 presenting the highest induction of APP expression and *APOE* ε2 the lowest (Huang et al., 2017). Accordingly, *APOE* ε4 represents an increased risk for AD, while *APOE* ε2 is protective against AD (Yu et al., 2014). APOE plays a role in metabolism regulation and it is known that its isoforms differently regulate glucose pathways (Keeney et al., 2015). It has been previously shown that *APOE ε4* decreases the levels of mitochondrial respiratory complexes, further linking APOE to mitochondrial metabolism (Chen et al., 2011). In addition, APOE has transcriptional factor activity as it binds to the promoter of genes related to trophic support, programmed cell death, microtubule disassembly, synaptic function, aging, and insulin resistance (Theendakara et al., 2016).

Considering the increased APOE level in MTL, the relevance of metabolic control in this region, as well as the relationship between APOE, Aβ, and tau, we summarize how differences in APOE expression could be related to MTL vulnerability to AD (Fig. 9). We believe that 1) the proteomic background, including higher APOE level together with 2) the high energy demand of MTL, impaired early in AD, make this region more susceptible to early triggers of AD. Previous work described the correlation between AD histopathological staging and the expression pattern of proteins that co-aggregate with plaques and tangles, as well as proteins involved in Aβ and tau homeostasis (Freer et al., 2016). These observations collectively suggest that a sum of factors might account for brain region vulnerability to AD and the whole picture needs to be elucidated.

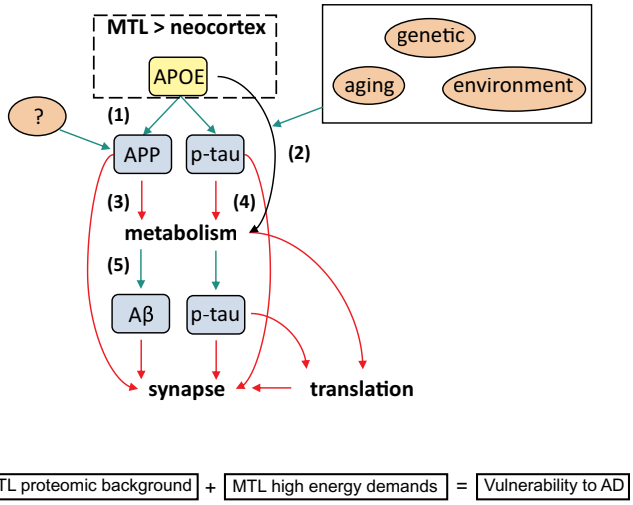

Fig. 9. Possible consequences of increased APOE levels in the MTL.
Scheme showing how differences in APOE expression could be related to MTL vulnerability to 1 CE) APOE stimulates APP transcription and tau phosphorylation; 2) APOE plays a role in metabolism regulation; 3) APP inhibits oxidative phosphorylation; 4) tau regulates insulin signaling; 5) hypometabolism increases Aβ levels and tau phosphorylation. Two additive effects, among others, would be involved in MTL vulnerability to AD. The endogenous proteomic background of MTL, especially its higher APOE level, might confer susceptibility to early triggers of AD (Aβ, tau, others); and the high energy demands of MTL, which is impaired early in the disease course, make this region more vulnerable to the toxic effects of Aβ and tau.

4.5. Comparison of proteomic studies in AD reveals overlapping proteins and pathways

A recent review of proteomic studies in AD reported low reproducibility between distinct works (Moya-Alvarado et al., 2016). However, we compared our results with two other proteomic datasets reported earlier, and 275 overlapping DEPs between at least two studies were found, furthermore, 85% of the common proteins showed concordant expression level changes across studies. The low number of overlapping proteins (24) between the three studies might be due to the anatomical divergence between the analyzed brain regions. Taken together, these results indicate that there is a certain degree of overlap between various proteomic studies, and most probably, the intersection denotes important proteins to AD pathology. A recent work that compared the results from three transcriptomic studies on the human hippocampus in AD (Hargis and Blalock, 2017), revealed that the overlapping up- and down-regulated genes are involved mainly in cell adhesion and platelet aggregation, and in energy metabolism and synaptic processes, respectively. This is in great agreement with the enrichment analysis results we got for the overlapping proteins between proteomic studies in AD (Fig. 7B). This further strengthens the view that there are key proteins and pathways commonly identified by distinct transcriptomic/proteomic studies which are of importance to AD etiology.

5. Conclusions

This work provides a description of the proteomic changes during AD progression in brain regions early and late affected by tau pathology. We identified peculiar mechanisms to each region during AD progression, but also found processes that are shared between regions possibly representing fundamental features involved in disease etiology. Based on the different proteomic signatures of MTL and neocortex, we contextualized brain region vulnerability to AD with the current Aβ/tau paradigm. In summary, this work provides insights into how distinct brain regions behave in health and during the course of AD. The results found strengthen the view that the differential proteomic background of various brain areas might be related to their implication in AD. In addition, we reinforce that the series of events leading to AD should be investigated at the whole brain level since the inherent characteristics of each brain region might be related to specific molecular alterations during disease. Future studies spanning more areas are needed to better clarify the cascade of events involved in AD and why particular brain regions are affected first by certain neurodegenerative diseases.

Supplementary data to this article can be found online at https://doi.org/10.1016/j.nbd.2019.104509.

Funding

A joint grant from the South Swedish healthcare sector Region Skåne and the National Research Council, Brazil supported this study. We thank the financial support from the Coordination of Improvement of Higher Education (CAPES) and Hungarian Brain Research Program (2017-1.2.1-NKP-2017-00002).

Availability of data and materials

The mass spectrometry proteomics data have been deposited to the ProteomeXchange Consortium via the PRIDE partner repository with the dataset identifier PXD010138.

Authors' contributions

CFM conceived the original idea. CFM and MR conceived and planned the experiments. CFM performed the experiments of entorhinal, parahippocampal and temporal cortex, MK performed the experiments of frontal cortex. MR advised mass spectrometry analysis and performed PRM analysis. IP advised statistical procedures. IP, CFM, MR, and MK contributed to define the statistical workflow. CFM analyzed data and performed biological interpretation. CFM draft the article. MR, GBD, FCSN, GMV, PD, TH, ER, and MP revised the article. LC and TH carried out the histopathological examination of samples and contributed to manuscript drafting. MP, ER provided samples and contributed to manuscript drafting. PD participated in the conceivement of the project and contributed to manuscript drafting. MR, GBD, FCSN, and GMV supervised the work.

Ethics approval

Ethical approval was given by the Semmelweis University Regional Committee of Science and Research Ethics (No. 32/1992/TUKEB) and the Committee of Science and Research Ethics of the Ministry of Health in Hungary (No. 6008/8/2002/ETT).

Consent for publication

All authors have approved of the contents of this manuscript and provided consent for publication.

Competing interests

The authors declare that they have no competing interests.

Acknowledgments

The authors thank Magdolna Toronyay-Kasztner and Alexander Rappensberger for technical assistance, Krzysztof Pawlowski for performing IPA analysis and Zsolt Horváth for help in the preparation of illustrations.

References

Alzheimer's Association, A. S, 2017. 2017 Alzheimer's disease facts and figures. Alzheimer's & Dementia 13, 325–373.
Bossers, K., et al., 2010. Concerted changes in transcripts in the prefrontal cortex precede neuropathology in Alzheimer's disease. Brain 133, 3699–3723.
Braak, H., Braak, E., 1991. Neuropathological stageing of Alzheimer-related changes. Acta Neuropathol. 82, 239–259.
Chen, H.K., et al., 2011. Apolipoprotein E4 domain interaction mediates detrimental effects on mitochondria and is a potential therapeutic target for Alzheimer disease. J. Biol. Chem. 286, 5215–5221.
Corder, E.H., et al., 1993. Gene dose of apolipoprotein E type 4 allele and the risk of Alzheimer's disease in late onset families. Science. 261, 921–923.
de Leon, M.J., et al., 2001. Prediction of cognitive decline in normal elderly subjects with 2-[18F]fluoro-2-deoxy-D-glucose/positron-emission tomography (FDG/PET). Proc. Natl. Acad. Sci. 98, 10966–10971.
Ding, Q., 2005. Ribosome dysfunction is an early event in Alzheimer's disease. J. Neurosci. 25, 9171–9175.
Freer, R., et al., 2016. A protein homeostasis signature in healthy brains recapitulates tissue vulnerability to Alzheimers disease. Sci. Adv. 2 (e1600947-e1600947).
Garcia-Esparcia, P., et al., 2017. Altered mechanisms of protein synthesis in frontal cortex in Alzheimer disease and a mouse model. Am. J. Neurodegener. Dis. 6, 15–25.
Gunawardana, C.G., et al., 2015. The human tau Interactome: binding to the Ribonucleoproteome, and impaired binding of the proline-to-leucine mutant at position 301 (P301L) to chaperones and the proteasome. Mol. Cell. Proteomics 14, 3000–3014.
Hargis, K.E., Blalock, E.M., 2017. Transcriptional signatures of brain aging and Alzheimer's disease: what are our rodent models telling us? Behav. Brain Res. 322, 311–328.
Hernández-Ortega, K., et al., 2015. Altered machinery of protein synthesis in Alzheimer's: from the nucleolus to the ribosome. Brain Pathol. 26, 593–605.
Hondius, D.C., et al., 2016. Profiling the human hippocampal proteome at all pathologic stages of Alzheimer's disease. Alzheimers Dement. 12, 654–668.
Hu, Y.-S., et al., 2017. Analyzing the genes related to Alzheimer's disease via a network and pathway-based approach. Alzheimers Res. Ther. 9.
Huang, Y.-W.A., et al., 2017. ApoE2, ApoE3, and ApoE4 differentially stimulate APP transcription and Aβ secretion. Cell 168, 427–441 (e21).
Hyman, B.T., et al., 2012. National Institute on aging–Alzheimer's association guidelines for the neuropathologic assessment of Alzheimer's disease. Alzheimers Dement. 8, 1–13.
Keeney, J.T.-R., et al., 2015. Human ApoE isoforms differentially modulate glucose and amyloid metabolic pathways in female brain: evidence of the mechanism of neuroprotection by ApoE2 and implications for Alzheimer's disease prevention and early intervention. J. Alzheimers Dis. 48, 411–424.
Kim, D.K., et al., 2018. Molecular and functional signatures in a novel Alzheimer's disease mouse model assessed by quantitative proteomics. Mol. Neurodegener. 13, 2.
Lachén-Montes, M., et al., 2017. Olfactory bulb neuroproteomics reveals a chronological perturbation of survival routes and a disruption of prohibitin complex during Alzheimer's disease progression. Sci. Rep. 7.
Lau, P., et al., 2013. Alteration of the microRNA network during the progression of Alzheimer's disease. EMBO Mol. Med. 5, 1613–1634.
Lauretti, E., et al., 2017. Glucose deficit triggers tau pathology and synaptic dysfunction in a tauopathy mouse model. Transl. Psychiatry 7 (e1020-e1020).
Liang, W.S., et al., 2007. Gene expression profiles in anatomically and functionally distinct regions of the normal aged human brain. Physiol. Genomics 28, 311–322.
Liang, W.S., et al., 2008. Alzheimer's disease is associated with reduced expression of energy metabolism genes in posterior cingulate neurons. Proc. Natl. Acad. Sci. 105, 4441–4446.
Lopez Sanchez, M.I.G., et al., 2017. Amyloid precursor protein drives down-regulation of mitochondrial oxidative phosphorylation independent of amyloid beta. Sci. Rep. 7.
Marciniak, E., et al., 2017. Tau deletion promotes brain insulin resistance. J. Exp. Med. 214, 2257–2269.
Martin, B., et al., 2008. iTRAQ analysis of complex proteome alterations in 3xTgAD Alzheimer's mice: understanding the Interface between physiology and disease. PLoS ONE 3, e2750.
Masters, C.L., et al., 2015. Alzheimer's disease. Nat. Rev. Disease Prim. 15056.
Matarin, M., et al., 2015. A genome-wide gene-expression analysis and database in transgenic mice during development of amyloid or tau pathology. Cell Rep. 10, 633–644.
McKetney, J., et al., 2019. Proteomic atlas of the human brain in Alzheimer's disease. J. Proteome Res. 18, 1380–1391.
Meier, S., et al., 2016. Pathological tau promotes neuronal damage by impairing ribosomal function and decreasing protein synthesis. J. Neurosci. 36, 1001–1007.
Miyashita, A., et al., 2014. Genes associated with the progression of neurofibrillary tangles in Alzheimer's disease. Transl. Psychiatry 4 (e396-e396).
Mosconi, L., 2013. Glucose metabolism in normal aging and Alzheimer's disease: methodological and physiological considerations for PET studies. Clin. Transl. Imaging 1, 217–233.
Mosconi, L., et al., 2008. Hippocampal hypometabolism predicts cognitive decline from normal aging. Neurobiol. Aging 29, 676–692.
Moya-Alvarado, G., et al., 2016. Neurodegeneration and Alzheimer's disease (AD). What can proteomics tell us about the Alzheimer's brain? Mol. Cell. Proteomics 15, 409–425.
Nelson, P.T., et al., 2007. Clinicopathologic correlations in a large Alzheimer disease center autopsy cohort. J. Neuropathol. Exp. Neurol. 66, 1136–1146.
O'Connor, T., et al., 2008. Phosphorylation of the translation initiation factor eIF2α increases BACE1 levels and promotes Amyloidogenesis. Neuron 60, 988–1009.
Palkovits, M., 1973. Isolated removal of hypothalamic or other brain nuclei of the rat. Brain Res. 59, 449–450.
Polydoro, M., et al., 2013. Soluble pathological tau in the entorhinal cortex leads to presynaptic deficits in an early Alzheimer's disease model. Acta Neuropathol. 127, 257–270.
Rakic, P., 2009. Evolution of the neocortex: a perspective from developmental biology. Nat. Rev. Neurosci. 10, 724–735.
Rezeli, M., et al., 2015. Quantification of total apolipoprotein E and its specific isoforms in cerebrospinal fluid and blood in Alzheimer's disease and other neurodegenerative diseases. EuPA Open Proteom. 8, 137–143.
Rhein, V., et al., 2009. Amyloid- and tau synergistically impair the oxidative phosphorylation system in triple transgenic Alzheimer's disease mice. Proc. Natl. Acad. Sci. 106, 20057–20062.
Savas, J.N., et al., 2017. Amyloid accumulation drives proteome-wide alterations in mouse models of Alzheimer's disease-like pathology. Cell Rep. 21, 2614–2627.
Scheff, S.W., et al., 2006. Hippocampal synaptic loss in early Alzheimer's disease and mild cognitive impairment. Neurobiol. Aging 27, 1372–1384.
Schonberger, S.J., et al., 2001. Proteomic analysis of the brain in Alzheimer's disease: molecular phenotype of a complex disease process. Proteomics 1, 1519.
Seyfried, N.T., et al., 2017. A multi-network approach identifies protein-specific co-expression in asymptomatic and symptomatic Alzheimer's disease. Cell Syst. 4, 60–72 (e4).
Shevchenko, G., et al., 2012. Longitudinal characterization of the brain proteomes for the Tg2576 amyloid mouse model using shotgun based mass spectrometry. J. Proteome Res. 11, 6159–6174.
Shi, Y., et al., 2017. ApoE4 markedly exacerbates tau-mediated neurodegeneration in a mouse model of tauopathy. Nature 549, 523–527.
Skogseth, R., et al., 2017. Accuracy of clinical diagnosis of dementia with Lewy bodies versus neuropathology. J. Alzheimers Dis. 59, 1139–1152.
Squire, L.R., et al., 2004. The medial temporal lobe. Annu. Rev. Neurosci. 27, 279–306.
Sultana, R., et al., 2010. Redox proteomic analysis of carbonylated brain proteins in mild cognitive impairment and early Alzheimer's disease. Antioxid. Redox Signal. 12, 327–336.

Terry, R.D., et al., 1991. Physical basis of cognitive alterations in alzheimer's disease: synapse loss is the major correlate of cognitive impairment. Ann. Neurol. 30, 572–580.
Thal, D.R., et al., 2002. Phases of Aβ-deposition in the human brain and its relevance for the development of AD. Neurology 58, 1791–1800.
Theendakara, V., et al., 2016. Direct Transcriptional effects of Apolipoprotein E. J. Neurosci. 36, 685–700.
Triplett, J.C., et al., 2016. Quantitative Phosphoproteomic analyses of the inferior parietal lobule from three different pathological stages of Alzheimer's disease. J. Alzheimers Dis. 49, 45–62.
Virok, D.P., et al., 2011. Protein Array based Interactome analysis of amyloid-β indicates an inhibition of protein translation. J. Proteome Res. 10, 1538–1547.
Vizcaíno, J.A., et al., 2015. 2016 update of the PRIDE database and its related tools. Nucleic Acids Res. 44, D447–D456.
Walsh, D.M., et al., 2002. Naturally secreted oligomers of amyloid β protein potently inhibit hippocampal long-term potentiation in vivo. Nature 416, 535–539.
Wisniewski, J.R., et al., 2009. Universal sample preparation method for proteome analysis. Nat. Methods 6, 359–362.
Xu, J., et al., 2019. Regional protein expression in human Alzheimer's brain correlates with disease severity. Commun. Biol. 2, 43.
Yoshiyama, Y., et al., 2007. Synapse loss and microglial activation precede tangles in a P301S Tauopathy mouse model. Neuron 53, 337–351.
Yu, J.-T., et al., 2014. Apolipoprotein E in Alzheimer's disease: an update. Annu. Rev. Neurosci. 37, 79–100.
Zahid, S., et al., 2014. Differential expression of proteins in brain regions of Alzheimer's disease patients. Neurochem. Res. 39, 208–215.
Zelaya, M.V., et al., 2015. Olfactory bulb proteome dynamics during the progression of sporadic Alzheimer's disease: identification of common and distinct olfactory targets across Alzheimer-related co-pathologies. Oncotarget 6.